PROCEEDINGS OF SCIENCE

Muon $g-2$: Lattice calculations of the hadronic vacuum polarization

Simon Kuberski

Theoretical Physics Department, CERN, 1211 Geneva 23, Switzerland
Helmholtz-Institut Mainz, Johannes Gutenberg-Universität Mainz, Germany
GSI Helmholtz Centre for Heavy Ion Research, Darmstadt, Germany

E-mail: simon.kuberski@cern.ch

The experimental uncertainty on the anomalous magnetic moment of the muon has been significantly reduced with the recent results of the Fermilab $g-2$ experiment, and a further reduction is expected in the near future. The precision of the Standard Model prediction needs to improve correspondingly to increase the sensitivity of tests for physics beyond the Standard Model. The largest uncertainty is due to contributions from the strong interaction, in particular the hadronic vacuum polarization (HVP) contribution.

Lattice QCD calculations have the potential to provide precise ab initio predictions of the HVP contribution. We review the state of lattice QCD calculations, focusing on the dominant sources of uncertainty that need to be controlled to provide results with sub-percent precision.

The 40th International Symposium on Lattice Field Theory (Lattice 2023)
July 31st - August 4th, 2023
Fermi National Accelerator Laboratory

PoS(LATTICE2023)125

1. Introduction

A long-standing tension between the Standard Model (SM) prediction and the experimentally measured value of the anomalous magnetic moment of the muon a_μ has sparked both theoretical and experimental efforts, hoping to enhance the significance of the tension in the search for physics beyond the Standard Model of particle physics.

The anomalous magnetic moment of a lepton l is defined as the deviation of its g-factor from its classical value $g = 2$,

$$a_l = \frac{1}{2}(g_l - 2), \tag{1}$$

due to quantum loop corrections from QED, electroweak and strong interactions and possibly due to physics beyond the Standard Model. Contributions to a_l induced by heavy particles with mass M which are not part of the Standard Model enter proportionally to m_l^2/M^2 and are thus enhanced by four orders of magnitude, when considering a_μ instead of a_e. The anomalous magnetic moments of the electron and the muon have been determined to very high precision, i.e., to 0.11 ppb [1] and 0.19 ppm [2–4], respectively. The uncertainty of a_μ is expected to reduce further when the data from Runs 4-6 of the Fermilab $g-2$ experiment will be included in the experimental average.

To test for physics beyond the Standard Model, SM predictions have to be known at the same level of precision. Whereas QED [5, 6] and electroweak [7, 8] contributions to a_μ are known to a precision that exceeds the experimental one by far, the uncertainty of the leading-order hadronic contributions to a_μ dominate the theory uncertainty. These are the hadronic vacuum polarization (HVP) contribution $a_\mu^{\rm hvp}$, entering at order α^2, and the hadronic light-by-light scattering (HLBL) contribution $a_\mu^{\rm hlbl}$ at $\mathrm{O}(\alpha^3)$. Whereas, thanks to recent work, SM predictions of $a_\mu^{\rm hlbl}$ approach the precision target of 10%, also in the lattice calculations of [9–12], the situation is less favorable in the case of $a_\mu^{\rm hvp}$, where a target uncertainty of about 0.2% will be needed to make full use of the advancements on the experimental side.

Traditionally, $a_\mu^{\rm hvp}$ has been computed from experimental data for the cross-section $\sigma(e^+e^- \to \text{hadrons})$ and a dispersion relation via,

$$a_\mu^{\rm hvp} = \left(\frac{\alpha m_\mu}{3\pi}\right)^2 \int_{m_{\pi^0}^2}^{\infty} \mathrm{d}s \frac{\hat{K}(s)}{s^2} R(s), \qquad R(s) = \frac{\sigma(e^+e^- \to \text{hadrons})}{4\pi\alpha^2/(3s)}, \tag{2}$$

where $\hat{K}(s)$ is a known QED kernel function [13]. The precision of the evaluation in the White Paper of the Muon $g-2$ theory initiative [14] based on [15–21] is limited by a tension between the two most precise experimental data sets by the KLOE and BABAR experiments in the $e^+e^- \to \pi^+\pi^-$ channel that contributes dominantly to $a_\mu^{\rm hvp}$. A recent new measurement of this contribution with the CMD-3 detector [22] is in tension with all previously obtained results and would potentially lead to an inflation of uncertainties, when included in the analysis. An alternative determination based on μe scattering at the MUonE experiment [23] is aiming at a precision at the level of 0.3%. The data taking can only be started after the long shutdown 3 at CERN in 2029.

Lattice QCD provides the optimal framework to compute the hadronic contributions to a_μ from first principles. Recent work has shown that precise results can be obtained, keeping all sources of uncertainty under control. In the following, we briefly recapitulate how $a_\mu^{\rm hvp}$ is computed

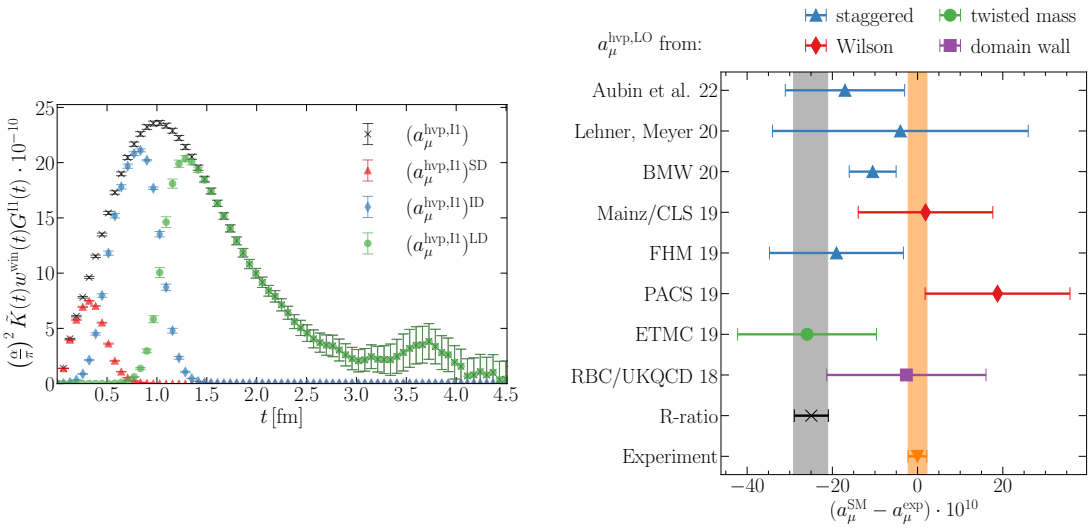

Figure 1: Left: The integrand of eq. (8) for the isovector correlation function on an ensemble at physical pion mass [24]. The black crosses show the full integrand whereas the colored data show the integrands of the three windows observables, based on eq. (11). Right: Comparison of SM predictions for a_μ with the experimental world average [2–4]. The SM predictions differ only in the leading-order HVP contribution from the R-ratio [15–21] or lattice QCD [25–32]. The lattice QCD results are grouped by fermion discretization.

from lattice QCD and collect recent results for $a_\mu^{\rm hvp}$ and several sub-contributions. We point out the dominant and subleading sources of uncertainty and how they are addressed in modern calculations.

2. The HVP contribution from lattice QCD

The natural starting point for the computation of the HVP in Euclidean space-time is the polarization tensor,

$$\Pi_{\mu\nu}(Q) = \int \mathrm{d}^4x\, \mathrm{e}^{iQ\cdot x} \langle j_\mu^{\rm em}(x)\, j_\nu^{\rm em}(0)\rangle = (Q_\mu Q_\nu - \delta_{\mu\nu}Q^2)\Pi(Q^2), \tag{3}$$

based on the two-point function of the hadronic part of the electromagnetic current,

$$j_\mu^{\rm em} = \frac{2}{3}\bar{u}\gamma_\mu u - \frac{1}{3}\bar{d}\gamma_\mu d - \frac{1}{3}\bar{s}\gamma_\mu s + \frac{2}{3}\bar{c}\gamma_\mu c - \frac{1}{3}\bar{b}\gamma_\mu b + \frac{2}{3}\bar{t}\gamma_\mu t\,. \tag{4}$$

As pointed out in [33], a lattice calculation of the momentum dependent hadronic tensor allows one to compute the leading-order HVP contribution to the muon $g-2$ via

$$a_\mu^{\rm hvp} = \left(\frac{\alpha}{\pi}\right)^2 \int_0^\infty \mathrm{d}Q^2 f(Q^2)\hat{\Pi}(Q^2), \qquad \text{with} \quad \hat{\Pi}(Q^2) = 4\pi^2\left[\Pi(Q^2) - \Pi(0)\right] \tag{5}$$

where $f(Q^2)$ is a known analytic function that encodes (infinite volume) QED and depends on the lepton mass m_μ. The most recent lattice calculations make use of the time-momentum representation (TMR) to compute $a_\mu^{\rm hvp}$. As first shown in [34] the subtracted vacuum polarization function $\hat{\Pi}$ may

be written in terms of the spatially-summed, zero-momentum vector two-point correlation function

$$G(t) = -\frac{a^3}{3}\sum_{k=1}^{3}\sum_{\vec{x}}\left\langle j_k^{\mathrm{em}}(t,\vec{x})\, j_k^{\mathrm{em}}(0)\right\rangle , \tag{6}$$

via

$$\hat{\Pi}(Q^2) = \frac{4\pi^2}{Q^2}\int_0^\infty \mathrm{d}t\, G(t)\left[Q^2t^2 - 4\sin^2\left(\frac{1}{2}Qt\right)\right] . \tag{7}$$

By switching the order of integration over imaginary time and momentum in eq. (5), one obtains

$$a_\mu^{\mathrm{hvp}} := \left(\frac{\alpha}{\pi}\right)^2\int_0^\infty dt\, G(t)\widetilde{K}(t), \tag{8}$$

with an analytic QED kernel function $\widetilde{K}(t)$ [35] that gives weight to the long-distance regime of the correlation function.

Performing the Wick contractions of the two currents in eq. (6) gives rise to quark-connected and quark-disconnected correlation functions. In isospin-symmetric QCD, these are conventionally written as

$$G(t) = \frac{5}{9}G_{\mathrm{l}}(t) + \frac{1}{9}G_{\mathrm{s}}(t) + \frac{4}{9}G_{\mathrm{c}}(t) + \frac{1}{9}G_{\mathrm{b}}(t) + G_{\mathrm{disc}}(t) . \tag{9}$$

The top quark contribution is neglected here because it is not accessible on the lattice. It can be computed in perturbation theory but is too small to be relevant at the current level of uncertainty. There exists one lattice result [36] for the bottom quark contribution, to which perturbation theory is also applicable. The term $G_{\mathrm{disc}}(t)$ collects all quark-disconnected contributions. In the decomposition into isovector and isoscalar contributions,

$$G^{\mathrm{I1}}(t) = \frac{1}{2}G_{\mathrm{l}}(t), \qquad G^{\mathrm{I0}}(t) = \frac{1}{18}G_{\mathrm{l}}(t) + \frac{1}{9}G_{\mathrm{s}}(t) + \frac{4}{9}G_{\mathrm{c}}(t) + \frac{1}{9}G_{\mathrm{b}}(t) + G_{\mathrm{disc}}(t), \tag{10}$$

the finite-volume effects of light-connected and disconnected contributions largely cancel within G^{I0} [29], facilitating the overall correction for these effects.

The typical shape of the integrand in eq. (8) for the isovector contribution at physical value of the light quark mass is displayed by the black crosses in Figure 1. Whereas the correlation function decreases exponentially with increasing time separation t, the QED kernel function $\tilde{K}$ increases polynomially [35]. The interplay of the two results in a large contribution of time separations beyond 1.5 fm, complicating the precise determination of the integral due to a signal-to-noise problem in $G^{\mathrm{I1}}(t)$. The contribution from times beyond 4 fm is numerically small. At the same time, the integrand probes very short distances where the correlator may be determined precisely but is affected by significant cutoff effects.

In [34], it has been suggested to split the integration in three different contributions at short, intermediate and long distances. Smooth window functions in Euclidean time, defined by

$$\begin{aligned} w^{\mathrm{SD}}(t;t_0;t_1) &= [1-\Theta(t,t_0,\Delta)], & w^{\mathrm{ID}}(t;t_0;t_1) &= [\Theta(t,t_0,\Delta)-\Theta(t,t_1,\Delta)], \\ w^{\mathrm{LD}}(t;t_0;t_1) &= \Theta(t,t_1,\Delta), & \Theta(t,t',\Delta) &:= \tfrac{1}{2}\left(1+\tanh[(t-t')/\Delta]\right) \end{aligned} \tag{11}$$

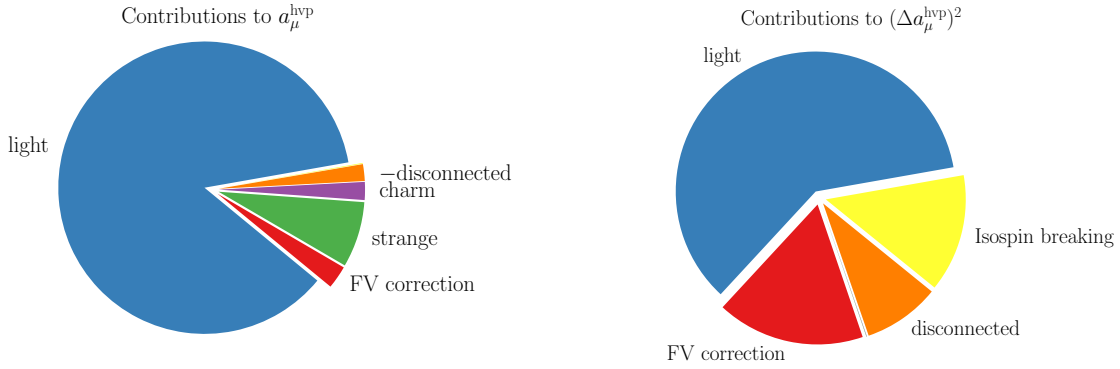

Figure 2: Contributions to the value (left) and the squared uncertainty (right) of $a_\mu^{\rm hvp}$ based on the calculation in [30]. The quark-disconnected contribution is negative.

with the parameters $t_0 = 0.4\,\text{fm}$, $t_1 = 1.0\,\text{fm}$ and $\Delta = 0.15\,\text{fm}$ have been introduced in [25] to smoothly separate the three regions. So-called window observables can be defined by inserting one of these functions $w^X(t;t_0;t_1)$ in the integrand of eq. (8). The resulting integrands add up to the integrand of eq. (8) and are shown by colored markers in Figure 1. The window observables aid in untangling and confirming control over various sources of systematic uncertainty, both at short and long distances. Recent result the for short and intermediate distance contributions will be discussed in section 5.

3. Results for $a_\mu^{\rm hvp}$

The right panel of Figure 1 compares Standard Model predictions for the leading-order HVP contribution to a_μ with the current world average for the experimentally determined $a_\mu^{\rm exp}$ from [2–4]. The black cross and gray error band denote the White Paper average from [14], where $a_\mu^{\rm hvp}$ has been evaluated using data-driven dispersive methods from the R-ratio and perturbative QCD [15–21]. A $5.1\,\sigma$ tension is found when comparing this result with $a_\mu^{\rm exp}$.

The colored data points are obtained by using a lattice QCD result for $a_\mu^{\rm hvp}$, instead of the White Paper average. They show the most recent results of eight collaborations [25–32] using four different classes of fermion discretizations. Whereas most results have an uncertainty of about 2%, the result marked by 'BMW 20' from [30] has reached sub-percent precision. As visible from the figure, this result is in between the experimental result and the SM prediction from the R-ratio. A further, independent lattice QCD result, preferably using a different fermion action, is needed to make a clear statement concerning the current discrepancy between two types of SM predictions.

The computation of $a_\mu^{\rm hvp}$ on the lattice to sub-percent precision is challenging due to a number of sources of uncertainty that have to be addressed appropriately in order to claim full control over the final uncertainty. In Figure 2 we illustrate the weight of each contribution to $a_\mu^{\rm hvp}$ and its uncertainty, based on the result from [30]. On the left hand side, the contribution to the central value is shown, based on the decomposition in eq. (9). About 90% of the final value is due to the light-connected contribution. Quark flavors with larger mass contribute less because the correlation function decays more rapidly. The quark-disconnected contribution is negative and has a size of

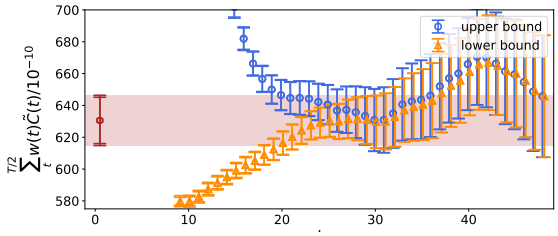

Figure 3: Bounding method applied to the local vector current correlation function. Figure taken from [37].

about 2% of the total. As discussed above, finite-volume effects in the flavor-decomposition mostly affect the light-connected and disconnected contributions.

On the right hand side of the figure, the contributions to the squared uncertainty of a_μ^{hvp} are shown. Since the result of [30] has reached sub-percent precision already, the pie chart gives an indication of the sources of uncertainty that have to be addressed in order to further improve the precision. Again, the dominant contribution comes from the light-connected contribution, containing the statistical uncertainty as well as the systematic uncertainty from the continuum extrapolation. The other three major contributions to the uncertainty are the correction for finite-volume effects, the effects due to isospin breaking and the quark-disconnected contribution.

4. Dominant sources of uncertainty

In the following, we will describe the methods that are currently being used to reduce and control the major sources of uncertainty in the calculation of a_μ^{hvp}.

4.1 Controlling the long-distance tail

The attainable statistical precision in the light-connected (or, equivalently, isovector) contribution has been the dominant source of uncertainty of many lattice QCD calculations of a_μ^{hvp}. A dramatic improvement in precision is achieved by combining theoretical constraints on the shape of the long-distance tail of the isovector correlation function with the use of optimized estimators in its computation.

Writing the spectral decomposition of the two-point correlation function as

$$G^{\mathrm{I1}}(t) = \sum_{n=0}^{N} \frac{Z_n}{2E_n} \mathrm{e}^{-E_n t} + \mathrm{O}(\mathrm{e}^{-E_{N+1} t}), \tag{12}$$

with the (positive) overlap factors Z_n and the finite-volume energies E_n, lower and upper bounds on the correlation function at Euclidean time t are given by [25, 38, 39]

$$0 \le G^{\mathrm{I1}}(t) \le G^{\mathrm{I1}}(t_c)\mathrm{e}^{-E_0(t-t_c)}, \qquad t \ge t_c\,. \tag{13}$$

The lower bound is based on the positivity of the correlation function and may be further tightened, making use of the fact that the correlation function in the long-distance regime decays more slowly than at short distances $\ll t_c$ [25, 29]. The upper bound relies on an estimate of the ground state energy in finite volume that, when not known from data, has to be estimated conservatively enough

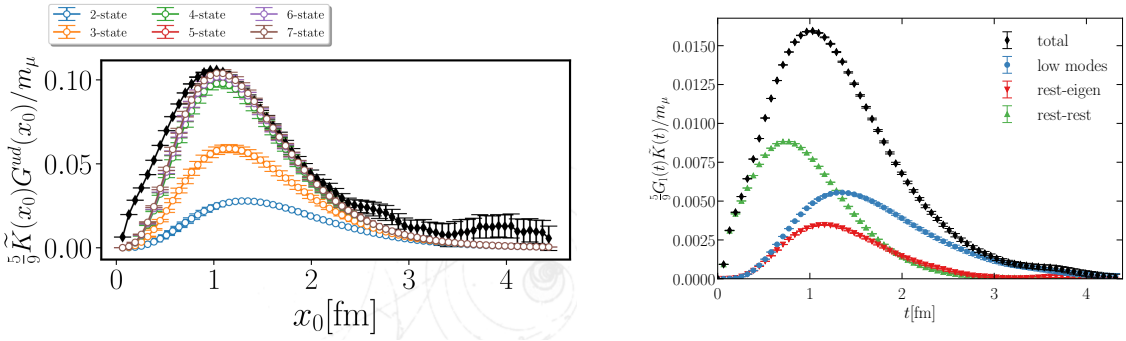

Figure 4: Left: Reconstruction of the integrand of the isovector contribution based on n $\pi\pi$ states. The black diamonds show the corresponding integrand from stochastic sources, as also shown in Figure 1. Taken from [40]. Right: The same (blinded) integrand but computed using low-mode averaging. The black diamonds are the sum of the three colored contributions and the blue circles show the all-to-all evaluation based on 800 low modes of the Dirac operator.

such that no model dependence is introduced when applying the bounds. As soon as both bounds agree with each other, the integration to infinite distances in eq. (8) may be performed using either of the bounds instead of the data itself. A example for this procedure is shown in Figure 3, taken from [37]. A reduction of the error by a factor of 2 is reported by the authors.

A further significant reduction of uncertainty can be achieved if several of the lowest states contributing to the spectral decomposition in eq. (12) are known. The corresponding finite-volume overlap factors and energies may be computed in a dedicated spectroscopy analysis in the isovector channel, as done in [29, 37, 41] The states coupling to the isovector current are mostly $\pi\pi$ states. In [37] it was found that 4π states seem to have a negligible overlap with the current, even though their energies are among the smallest in the spectral decomposition. Reconstructing the correlation function from the lowest-lying states eliminates the signal-to-noise problem completely, since the error of the reconstructed correlation function grows only linearly, as opposed to exponentially. This is illustrated in the left-hand panel of Figure 4, taken from [40], which shows that four $\pi\pi$ states are sufficient to saturate the isovector correlation starting at $t \gtrsim 1.5$ fm in a $(6.1\,\text{fm})^3$ spatial volume at physical pion mass.

The use of advanced numerical procedures for the optimization of the estimator for $G^{\text{I1}}(t)$ is common to all recent results for a_μ^{hvp}. Using the lowest O(1000) eigenmodes of the hermitian Dirac operator, at physical pion mass and $m_\pi L \approx 4$, to construct an all-to-all estimator of the long-distance tail of $G^{\text{I1}}(t)$ [42–44] turns out to be significantly more efficient than sampling with stochastic or point sources. Figure 4 shows an application of LMA for the same integrand as the one shown in Figure 1. It is constructed by summing three contributions: The blue circles, labeled 'low modes' show an all-to-all evaluation of the correlation function in the subspace of the lowest 800 modes of the even-odd preconditioned hermitian Dirac-Wilson operator. One clearly sees that this contribution to the integrand dominates starting at a distance of about 1.5 fm, exactly where the signal-to-noise problem starts to hinder the precise estimation of the integrand. Whereas the all-to-all sampling of the correlation function in the space of these lowest eigenmodes does not solve the exponential deterioration of the signal, it reduces the coefficient of the growth significantly. The correlation function in the orthogonal complement of the low modes, indicated by green triangles

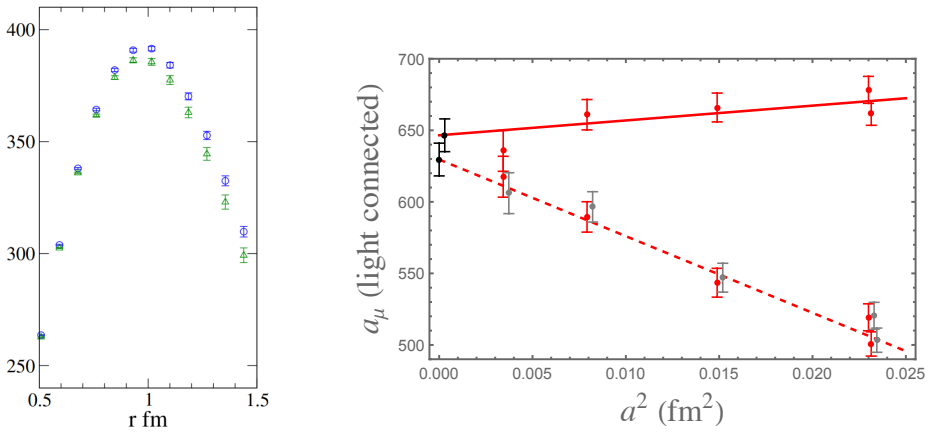

Figure 5: Left: Zoom into the integrands of the light-connected contribution on lattices with spatial volumes $(5.4\,\mathrm{fm})^3$ (triangles) and $(10.8\,\mathrm{fm})^3$ (circles). Taken from [27]. Right: Continuum limit of the light-connected contribution to a_μ^{hvp} with staggered quarks. The dashed line shows the continuum extrapolation without and the solid line the extrapolation with taste breaking corrections. Taken from [32].

in Figure 4 can be sampled stochastically. A number of methods exist to calculate the correlation function that contains propagators from both subspaces which may be small but has to be computed precisely to obtain a clean signal at large times. The solution of the Dirac equation can be accelerated by inexact inversions followed by a bias correction step [45–47].

The combination of some or all of the above techniques has enabled the community to compute the isovector contribution to a_μ^{hvp}, the largest source of statistical uncertainty, with a precision of a few per-mil at physical pion mass. We conclude this section by pointing out that new simulation paradigms such as multi-level integration [48, 49] offer promising solutions to the signal-to-noise problem, as demonstrated in [50] but not yet applied at large scales.

4.2 Finite-volume effects

The numerically largest contributions to the finite-volume effects of a_μ^{hvp} enter in the long-distance regime of the light-connected channel which is dominated by $\pi\pi$ states. A significant effect is also present for the quark-disconnected contribution, see section 6.1, and isospin breaking effects, cf. section 6.2. At the physical value of the pion mass and a conventional value of $m_\pi L = 4$, the finite volume shifts a_μ^{hvp} by about 3% compared to its infinite-volume counterpart. Any calculation aiming for sub-percent or even few per-mil precision therefore has to control the correction for finite-size effects at the 10% level or use volumes which are significantly larger than $(6\,\mathrm{fm})^4$.

Several approaches have been worked out to perform a correction for finite-size effects based on effective field theories. It has been found that next-to-leading (NLO) computations in chiral perturbation theory (χPT) can not fully describe finite-volume effects that are found in the data [27, 51] and that NNLO effects are significant [52–54]. An extension of the framework incorporates the ρ meson and photons [55–57].

The relation between the two-pion spectrum in finite volume and the timelike pion form factor can be used to compute the difference between finite and infinite-volume isovector correlation

functions based on a spectral decomposition [58–60]. This ansatz is expected to be particularly successful at large distances where only a few states contribute to the finite-volume correlation function. If no direct lattice calculation of the timelike pion form factor on the lattice is available, a Gounaris-Sakurai parametrization [61] of the form factor can be employed for the finite-volume correction [29, 35, 51, 62].

A generic, relativistic effective field theory of pions has been employed to compute finite-size and thermal effects on $a_\mu^{\rm hvp}$ in [63, 64]. It was suggested to approximate the forward Compton amplitude by the pion pole term which is determined by the electromagnetic pion form factor in the spacelike region.

Simulations in large volumes with spatial extents $L > 10\,\text{fm}$ [27, 30], followed by a small, model-dependent, correction to infinite volume can be used to minimize the model dependence of finite-volume corrections. Figure 5 shows the integrand of the light-connected contribution to $a_\mu^{\rm hvp}$ for two spatial volumes of $(5.4\,\text{fm})^3$ and $(10.8\,\text{fm})^3$ from [27]. A clear difference between the two can be resolved, already in the intermediate-distance region. While simulations with $L > 10\,\text{fm}$ are prohibitively expensive at fine lattice spacing, they may be carried out for coarser lattices, together with an assumption on the size of the cutoff effects for the finite-volume correction. This approach has been used by the BMW collaboration in [30] to correct from a reference volume with $L \approx 6.3\,\text{fm}$ and $T = \frac{3}{2}L$ to a volume of $(10.75\,\text{fm})^4$. The latter has been simulated at a single lattice spacing using an action with reduced taste-breaking effects.

4.3 The continuum limit

The systematic uncertainty associated with the continuum extrapolation can easily be the dominant source of uncertainty, as it is the case in the most precise calculation to date [30]. Whereas all of the lattice results in Figure 1 employ a setup where cutoff effects of $\mathrm{O}(a)$ are absent, higher-order cutoff effects and modifications of the leading a^2 behavior may induce significant systematic uncertainties since they may be difficult to constrain. The use of at least four values of the lattice spacing and a sufficiently large range of resolutions is mandatory to claim control over the continuum extrapolation in high-precision calculations of $a_\mu^{\rm hvp}$.

As pointed out in [65, 66], cutoff effects of $\mathrm{O}(a^2\log(a))$ can be expected already at the classical level of Symanzik effective theory (SymEFT) from the integration at very short distances in the TMR integral in eq. (8) and the interplay between correlation function and kernel function $\widetilde{K}(t)$. These may be efficiently eliminated from the computation by using perturbative QCD at these short distances, as already suggested in [34].

More worrisome in terms of potentially large corrections to a^2 scaling that might not be resolved at present-day lattice spacings are logarithmic modifications of the form $a^2 \to a^2[\bar{g}^2(1/a)]^{\hat{\gamma}_i}$ with the renormalized coupling $\bar{g}^2(1/a)$ and one-loop anomalous dimensions $\hat{\gamma}_i$. These effects are induced by quantum corrections in SymEFT. The dominantly contributing anomalous dimensions from Wilson-type and Domain Wall fermion actions have been computed in [67, 68] with the result that negative powers, which would slow down the approach to the continuum limit, have not been found. An extension to quark bilinears has been presented at this conference [69]. In view of the target precision it is mandatory to include this information in continuum extrapolations of precision observables, such as $a_\mu^{\rm hvp}$, or to test a generous range of anomalous dimensions if no information is available, as it is the case for staggered fermions.

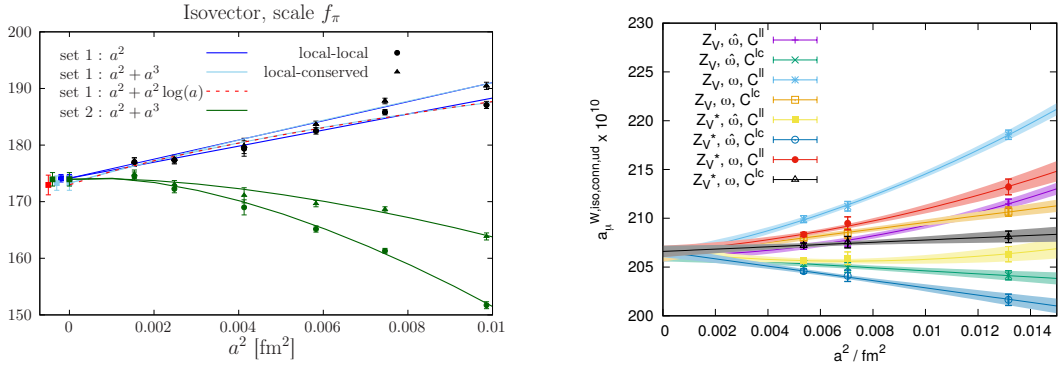

Figure 6: Continuum extrapolations of the isovector contribution to $(a_\mu^{\rm hvp})^{\rm ID}$. Each data set and the corresponding extrapolation is based on a specific choice to define the observable at finite lattice spacing. Left: At the SU(3) symmetric point from [70]. Right: At physical quark mass from [71].

For staggered quarks, another significant source of discretization effects is present in calculations of $a_\mu^{\rm hvp}$, namely taste-breaking effects that distort the pion spectrum at finite lattice spacing. Since non-linearities in the continuum extrapolation are introduced by the taste-breaking effects [32], a correction is conventionally applied prior to the continuum extrapolation, based on staggered χPT [28, 30, 32, 52]. On the right hand side of Figure 5 we show an example from a recent calculation [32] where the data is shown prior to the correction (lower data points) and after the correction. Care has to be taken in this step to ensure that all possible model dependence is appropriately accounted for in the estimation of the systematic uncertainty.

Various definitions of the observable at finite lattice spacing, differing by $O(a^2)$, have been applied when computing window observables. This approach serves a dual purpose: either as a cross-check ensuring that extrapolations coincide in the continuum limit [70] or through combined extrapolations that are constrained to be consistent in the continuum [71, 72]. Two of these extrapolations for the isovector contribution to the intermediate-distance window observable are shown in Figure 6. While this approach constrains cutoff effects in the valence sector, cutoff effects from the sea that are common to all data points are not better constrained.

4.4 Scale setting

Although a_μ is a dimensionless quantity it inherits a scale dependence from the conversion of the muon mass to lattice units in the QED kernel function $\widetilde{K}$. Denoting the scale setting quantity by Λ, we can write

$$\frac{\partial a_\mu^{\rm hvp}}{\partial \Lambda} = \left(\frac{\alpha}{\pi}\right)^2 \int_0^\infty dt\, G(t) \left(\frac{\partial}{\partial \Lambda} \widetilde{K}(t)\right), \tag{14}$$

and, as pointed out in [35], a relative uncertainty $\Delta\Lambda/\Lambda$ on the scale setting quantity leads to a contribution of $\Delta a_\mu^{\rm hvp}/a_\mu^{\rm hvp} \approx 1.8\,(\Delta\Lambda/\Lambda)$ to the uncertainty of $a_\mu^{\rm hvp}$. Ultimately, a scale determination at the per-mil level has to be performed to be able to reach the precision goal for $a_\mu^{\rm hvp}$. The spread of results for (ratios of) gradient flow scales reported in the recent FLAG report [73] is an indication that the control over all sources of uncertainty may not be sufficient, at present. Aiming at a complete calculation of $a_\mu^{\rm hvp}$ with sub-percent precision, the effect of isospin breaking has to be

included in the scale setting. The Ω baryon, not being affected at leading order by the effect of strong isospin breaking, has emerged as the preferred scale setting quantity for many collaborations. Here, the main difficulty is the reliable extraction of the ground state mass from the baryon correlation function.

Incorporating a generic scale dependent window function $w^X(t)$ into eq. (14) leads to

$$\frac{\partial (a_\mu^{\rm hvp})^X}{\partial \Lambda} = \left(\frac{\alpha}{\pi}\right)^2 \int_0^\infty dt\, G(t) \left[\left(\frac{\partial}{\partial \Lambda} w^X(t) \right) \widetilde{K}(t) + w^X(t) \left(\frac{\partial}{\partial \Lambda} \widetilde{K}(t) \right) \right] . \tag{15}$$

An analysis of the interplay of the window functions of eq. (11) with $\widetilde{K}$ shows that the short-distance window has barely any scale dependence. For the intermediate-distance window observable one finds $\Delta(a_\mu^{\rm hvp})^{\rm id}/(a_\mu^{\rm hvp})^{\rm id} \approx 0.5\,(\Delta\Lambda/\Lambda)$. The significantly reduced scale dependence of $(a_\mu^{\rm hvp})^{\rm ID}$ further facilitates the precise computation of this quantity from lattice QCD. Consequently, an enhanced scale dependence with respect to $a_\mu^{\rm hvp}$ is found for the long-distance window observable.

We note that high-precision comparisons and consistency checks between lattice QCD results can be performed if the same, appropriate scale setting quantity is used throughout. Since the lattice uncertainty on an experimentally known dimensionful quantity does not enter in this case, gradient flow scales seem to be best suited for these comparisons as they can be computed with negligible uncertainty at finite lattice spacing (as opposed to baryon masses or decay constants).

5. Euclidean time windows in the time-momentum representation

The three window quantities defined in eq. (11) are the ideal testbed to verify the control over the systematic effects, which have been outlined in the previous section, by comparison among lattice results. Whereas finite-size effects contribute significantly in the long-distance window, where also the loss of signal plays an important role, a computation of the short distance window observable will be mostly affected by the systematic uncertainty from taking the continuum limit. The intermediate distance window observable on the other hand is designed such that these systematic effects are suppressed and therefore allows to compute and compare lattice results with high precision.

The windows in Euclidean time of eq. (11) can be translated to momentum space, allowing for a calculation of the window observables from the R-ratio [30, 74] and a comparison with lattice results. Since the localized windows in Euclidean time are non-local in momentum space, it is non-trivial to ascribe possible discrepancies between the two approaches to a certain interval in momentum space. Different window observables than the ones of eq. (11) have been suggested in [32, 74, 75] to allow for a more detailed comparison with dispersive methods . The combination of several observables can also help to disentangle contributions from different energy regions, as outlined in [76, 77].

A complementary path for a direct comparison between lattice results and the experimentally determined R-ratio has been taken in [78] where the smeared R-ratio has been obtained from the lattice using reconstruction methods and compared to its experimental counter part. The authors report a three sigma tension in the ρ region with respect to the R-ratio evaluation of [20].

5.1 The intermediate-distance window

Significant progress has been made in the computation of the intermediate distance window observable in the past years. Four collaborations [30, 70–72] have performed a complete calculation of $(a_\mu^{\rm hvp})^{\rm ID}$ with uncertainties between 0.6% and 0.35% which are dominated by systematic uncertainties in all cases.[1] The four results agree with each other and thus provide a confirmation of the result of [30] in the intermediate distance region that makes up for about one third of $a_\mu^{\rm hvp}$. The results are denoted by filled colored symbols on the left hand side of Figure 7 together with an evaluation of the same quantity from the R-ratio [74].[2]

If the four lattice results are averaged, assuming a very conservative 100% correlation, a $3.8\,\sigma$ discrepancy with respect to the dispersive result is found [80]. This points towards underestimated systematic uncertainties in either of the two approaches. Since the finite-volume corrections for $(a_\mu^{\rm hvp})^{\rm ID}$ are smaller than the final uncertainties and four different quark actions have been used, it is challenging to find an explanation for a potential effect that would affect all lattice results similarly and lead to a shift of about 3.5%. We note that the inclusion of the recent result of the CMD-3 collaboration for the $e^+e^- \to \pi^+\pi^-$ cross section at low energies in the data-driven evaluation of $(a_\mu^{\rm hvp})^{\rm ID}$ would lead to a larger value that would be better compatible with lattice QCD [22]. A similar observation is made when τ spectral functions are used instead of e^+e^- results [81–83]. The current $3.8\,\sigma$ discrepancy in $(a_\mu^{\rm hvp})^{\rm ID}$ is about half of the difference between the White Paper average and the result of [30] for $a_\mu^{\rm hvp}$.

A recent result for the light-connected contribution to the intermediate distance window observable, $(a_\mu^{\rm hvp})^{\rm ID,l}$, from the R-ratio [84] can be compared to a larger number of lattice results for this dominant contribution to $(a_\mu^{\rm hvp})^{\rm ID}$, as shown on the right-hand side of Figure 7. We note that only one further independent set of gauge ensemble is added when including the additional results. The two most recent results are based on blinded analyses to prevent a human bias in view of the large number of previous results. The discrepancy between lattice and R-ratio is even larger for $(a_\mu^{\rm hvp})^{\rm ID,l}$ due to smaller uncertainties and the fact that no significant deviation is found in the sum of strange-connected and disconnected contributions [84]. This can be taken as indication that an insufficient description of lattice artefacts cannot be responsible for the large discrepancy as it would affect light-connected and strange-connected contributions in a similar manner.

All of the results shown in Figure 7 use the time-momentum representation to compute $(a_\mu^{\rm hvp})^{\rm ID,l}$. A calculation based on the Lorentz-covariant coordinate-space representation [85] has confirmed the result of [70] at a pion mass of 350 MeV [86]. It is expected that this representation is especially well suited for the combination with simulations in the master-field paradigm [87].

5.2 The short-distance window

The control of cutoff effects from small Euclidean distances is the main challenge in any computation of the short-distance window observable $(a_\mu^{\rm hvp})^{\rm SD}$. Therefore, a successful comparison of lattice results can provide an indication that these cutoff effects are fully under control. From

[1] The estimate for isospin breaking effects in the result of [72] is taken from [30].

[2] The open symbols denote the results from [25, 79] which are superseded by the recent results of the RBC/UKQCD and ETM collaborations. The differences with respect to their recent results are understood to be due to long continuum or chiral extrapolations, respectively.

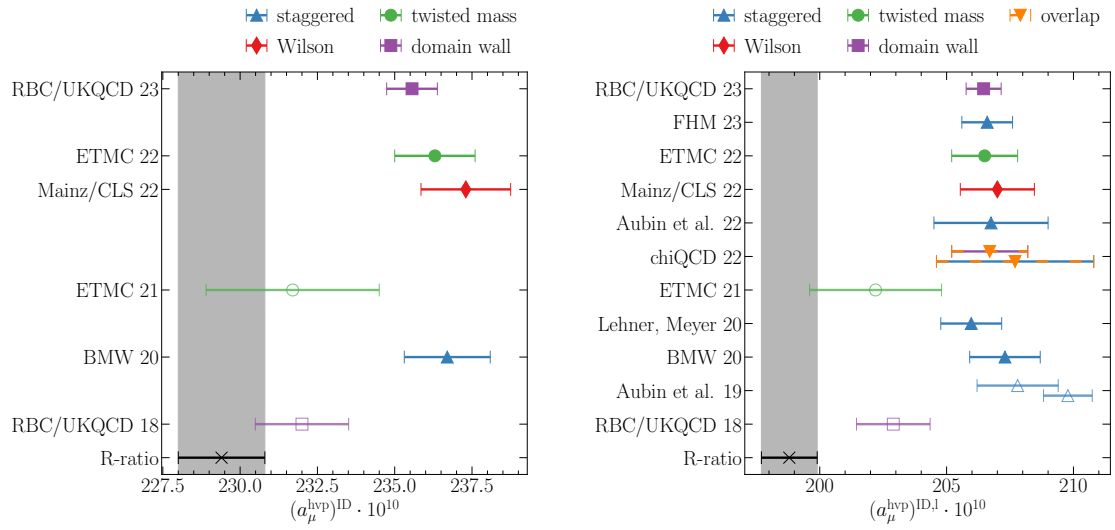

Figure 7: Left: Evaluations of $(a_\mu^{\rm hvp})^{\rm ID}$ from lattice QCD (colored points) [25, 30, 70–72, 79] and the R-ratio [74]. Right: Evaluations of $(a_\mu^{\rm hvp})^{\rm ID,l}$ from lattice QCD (colored points) [25, 30–32, 52, 70–72, 79, 88, 89] and the R-ratio [84]. chiQCD 22 [88] used overlap fermions in the valence sector and domain wall or staggered quarks in the sea. Superseded results are denoted by open symbols.

the phenomenological point of view, the comparison with an R-ratio evaluation might give further information concerning the origin of the current discrepancies.[3]

To date, one complete calculation [72] and one calculation of the light-connected part to $(a_\mu^{\rm hvp})^{\rm SD}$ [71] have been published. Both works employ three values of the lattice spacing in their combined continuum extrapolations of observables that have to agree in the continuum limit. The subtraction of tree-level cutoff effects [72] and the use of perturbation theory at order α_s^4 at very short distances [71] are used to tame or remove the potentially dangerous $O(a^2 \log(a))$ cutoff effects from the TMR integral. Whereas the two lattice results for $(a_\mu^{\rm hvp})^{\rm SD,l}$ agree, [72] finds a slight $1.4\,\sigma$ or 1.3% shift compared to the R-ratio evaluation of [74].

6. Subleading contributions

In addition to the dominant sources of uncertainty in lattice computations of $a_\mu^{\rm hvp}$, which primarily affect the light-connected contribution, two further significant sources of uncertainty can be identified on the right hand side of Figure 2, namely the one from the quark-disconnected contribution and from the inclusion of isospin breaking effects.

6.1 The quark-disconnected contribution

Neglecting charm quark contributions that have been shown to be small [72, 90], the quark-disconnected contribution can be formulated from differences of light and strange quark loops [91].

[3] An analysis of a phenomenological model for the R-ratio [34] suggests that, if the discrepancy in $(a_\mu^{\rm hvp})^{\rm ID}$ is due to an underestimate of the experimentally determined R-ratio in the region between 600 MeV and 900 MeV, a corresponding discrepancy of more than one percent would be expected in $(a_\mu^{\rm hvp})^{\rm SD}$ [70].

Therefore, this contribution vanishes at the SU(3) symmetric point of QCD, where it is a double zero in the quark mass difference $(m_\mathrm{l} - m_\mathrm{s})$ [29].

The estimation of this contribution is complicated by the fact that the noise of the quark-disconnected correlation function is constant whereas the correlation function falls off exponentially. At very long distances, it can be expected that the ratio of quark-disconnected and isovector correlation function approaches the asymptotic ratio $-\frac{1}{9}$ [62, 92]. Hence, the quark-disconnected contribution is foreseen to exhibit significant finite-volume effects, approximately $\frac{1}{9}$ those observed in the isovector channel. A cancellation of these effects is obtained in the isoscalar contribution, see eq. (10).

All-to-all propagators have to be computed in order to calculate the noisy quark-disconnected contribution. Several advanced algorithmic techniques are applied in this calculation, in addition to stochastic sources. As for the isovector correlation function, low modes of the Dirac operator and truncated solves [45] are used by many collaborations. Hierarchical probing [93], randomized sparse grids [94] or the hopping parameter expansion [95] for heavy quark contributions may lead to further improvements. Exploiting the structure of the correlation function by using the same set of sources for light and strange quark inversions has a significant impact on the quality of the signal [91]. The cancellation of noise in differences is further exploited in frequency-splitting estimators [96, 97]. A variant of the bounding method for the quark-disconnected [90] or the isoscalar contribution [98] can be used to enhance the precision of the TMR integral.

The precision of published evaluations of the disconnected contribution to a_μ^hvp is approaching the level of 10% [25, 28–30], not far from the target that is needed to reach per-mil precision for a_μ^hvp.

6.2 Isospin breaking effects

As soon as the precision of a Standard Model prediction has reached the 1% level, it is not sufficient to work in isospin symmetric QCD. Effects from strong-isospin breaking of order $(m_\mathrm{d} - m_\mathrm{u})/\Lambda_\mathrm{QCD}$ and from the inclusion of QED at order α, have to be considered, see, e.g., [99, 100].

Whereas simulations with dynamical QCD+QED [101, 102] and non-degenerate up and down quarks [103] are pursued in the context of computations of a_μ^hvp, most calculations of isospin breaking effects in a_μ^hvp are performed via a perturbative expansion in the isospin breaking parameters $\Delta m_f = m_f - \bar{m}$ and α around isospin symmetric QCD on isospin symmetric gauge ensembles [104, 105]. The benefit of being able to reuse existing gauge fields comes at the cost of having to compute a number of additional correlation functions. The combination of infinite-volume QED with finite-volume QCD has been proposed as alternative [25, 106, 107], similar to calculations of a_μ^hlbl [108, 109].

When $\mathrm{QED_L}$ [110] is used to formulate QED inside a finite box with periodic boundary conditions in the spatial directions, as it is the case in many calculations, the finite volume effects scale with $1/L^3$ [111], where L is the spatial extent. Given the conventionally used lattice sizes, this is sufficient in view of the precision targets since the finite-volume corrections affect a small contribution to a_μ^hvp. We note that the corrections are reduced to order $1/L^4$ when using $\mathrm{QED_C}$ [112, 113] or $\mathrm{QED_r}$ [100].

When comparing results for the isospin breaking effects in $a_\mu^{\rm hvp}$ or results for $a_\mu^{\rm hvp}$ in isopin symmetric QCD, care has to be taken since the separation of strong and QED isospin breaking effects is scheme dependent, as is the definition of the physical point in isosymmetric QCD. Whereas the differences between commonly used schemes are expected to be small, a common scheme prescription for the lattice community would significantly facilitate such comparisons in view of shrinking uncertainties [114]. The definition of the physical point in full QCD+QED is unambiguous.

No new results for isospin breaking effects in $a_\mu^{\rm hvp}$ have been published since the review in [115]. The effect of strong isospin breaking on the quark-connected contribution to $a_\mu^{\rm hvp}$ has been computed in [25, 26, 30, 31, 103]. The BMW collaboration found a large cancellation with the corresponding effect in the quark-disconnected contribution [30]. QED effects in the valence sector of quark-connected [25, 26, 30] and quark-disconnected [25, 30] have been computed by several collaborations, however, partly with 100% uncertainties. Only the calculation in [30] includes the effects of isospin breaking on sea quarks by computing diagrams that are suppressed by $\mathrm{SU}(3)_f$ or $1/N_c$ on boxes with spatial sizes of about 3 fm.

The complete calculation of [30] finds significant cancellations between different contributions to isospin breaking effects. Their final result of $0.5(1.4)\cdot 10^{-10}$ amounts to a sub per-mil effect on $a_\mu^{\rm hvp}$. In view of the difficulty of obtaining precise results for the isospin breaking effects, the smallness of the contribution is encouraging. However, more independent and precise results for the QED effects on valence and sea quarks are required before definite conclusions can be drawn. Progress in this direction has been made by several collaborations in the last years, see e.g. [70, 116, 117].

7. Conclusions

The upcoming decrease of experimental uncertainties for the anomalous magnetic moment of the muon after the analysis of the Run-4-6 data of the Fermilab Muon $g-2$ experiment calls for a reduction of theory uncertainties, especially for the HVP contribution. However, the disagreement between the data-driven results that were included in the White Paper average [14] and the most precise result from lattice QCD [30] has posed new questions concerning the SM prediction. A recent result [22] for the $e^+e^-\to\pi^+\pi^-$ cross-section at low energies that is incompatible with the two most precise previous results calls into question the control of systematic uncertainties of the data-driven calculation.

Lattice QCD computations have reached the stage where they are able to provide precise and reliable SM predictions for hadronic contributions to a_μ. Several independent results for $a_\mu^{\rm hvp}$ with sub-percent precision are needed to confirm that all sources of uncertainty are under control. Thanks to algorithmic advances, a deeper theoretical understanding of finite-volume and lattice spacing effects and a significant amount of invested computing resources, this goal is in reach.

For the intermediate distance window observable, the high degree of agreement between several independent results, as shown in Figure 7, leads to the conclusion that the discrepancy with respect to data-driven evaluations is firmly established. Given various cross-checks, a common systematic effect that affects all lattice results seems very unlikely.

It is desirable to obtain a similar level of agreement of lattice results for $a_\mu^{\rm hvp}$. With the ongoing reduction of statistical uncertainties, control of systematics becomes even more important. Calculations in very large boxes play an important role to reduce a possible model dependence of the finite-size correction. For upcoming results, the systematic uncertainty from the continuum extrapolation will likely become the dominant source of uncertainty. Since the accessible range of lattice spacings is limited, mostly due to critical slowing down towards the continuum limit [118], further significant improvements in the control of cutoff effects are difficult to achieve with simulations based on the Hybrid Monte Carlo algorithm. Better informed extrapolations based on SymEFT may help to reduce systematic uncertainties. In the meantime, combined continuum extrapolations of data from different fermion discretizations, having significantly different lattice artefacts, could constrain the approach to the continuum limit and thus lead to reduced systematic uncertainties.

Existing results indicate that isospin breaking effects in $a_\mu^{\rm hvp}$ are significantly smaller than 1%. More independent results are needed to confirm this conclusion. If a common scheme for QCD+QED is used in upcoming calculations, averages of sub-quantities, such as the light-connected contribution to $a_\mu^{\rm hvp}$, could be used to improve the global precision of $a_\mu^{\rm hvp}$ from lattice QCD.

Given the various tensions, blinded analyses have become standard to reduce the human bias in the analysis. We expect several new results for $a_\mu^{\rm hvp}$ and $(a_\mu^{\rm hvp})^{\rm LD}$ to be published in the next year. The outcome will be decisive in scrutinizing current tensions between Standard Model predictions and between theory and experiment.

Acknowledgements

I thank the organizers for the invitation to present a summary of the lattice calculations of $a_\mu^{\rm hvp}$, Harvey Meyer and Hartmut Wittig for a careful reading of the manuscript and all members of the Mainz lattice group for the fruitful collaboration in the last years. Calculations by Mainz/CLS were performed on HPC platforms at Mainz, JSC Jülich and HLRS Stuttgart. The support of the Gauss Centre for Supercomputing (GCS) and the John von Neumann-Institut für Computing (NIC) for projects CHMZ21 and CHMZ23 at JSC and project GCS-HQCD at HLRS is gratefully acknowledged. This project has received funding from the European Union's Horizon Europe research and innovation programme under the Marie Skłodowska-Curie grant agreement No 101106243.

References

[1] X. Fan, T. G. Myers, B. A. D. Sukra and G. Gabrielse, *Measurement of the Electron Magnetic Moment*, *Phys. Rev. Lett.* **130** (2023) 071801 [2209.13084].

[2] Muon g-2 collaboration, G. W. Bennett et al., *Final Report of the Muon E821 Anomalous Magnetic Moment Measurement at BNL*, *Phys. Rev. D* **73** (2006) 072003 [hep-ex/0602035].

[3] Muon g-2 collaboration, B. Abi et al., *Measurement of the Positive Muon Anomalous Magnetic Moment to 0.46 ppm*, *Phys. Rev. Lett.* **126** (2021) 141801 [2104.03281].

[4] Muon g-2 collaboration, D. P. Aguillard et al., *Measurement of the Positive Muon Anomalous Magnetic Moment to 0.20 ppm*, *Phys. Rev. Lett.* **131** (2023) 161802 [2308.06230].

[5] T. Aoyama, M. Hayakawa, T. Kinoshita and M. Nio, *Complete Tenth-Order QED Contribution to the Muon g-2*, *Phys. Rev. Lett.* **109** (2012) 111808 [1205.5370].

[6] T. Aoyama, T. Kinoshita and M. Nio, *Theory of the Anomalous Magnetic Moment of the Electron*, *Atoms* **7** (2019) 28.

[7] A. Czarnecki, W. J. Marciano and A. Vainshtein, *Refinements in electroweak contributions to the muon anomalous magnetic moment*, *Phys. Rev. D* **67** (2003) 073006 [hep-ph/0212229].

[8] C. Gnendiger, D. Stöckinger and H. Stöckinger-Kim, *The electroweak contributions to* $(g-2)_\mu$ *after the Higgs boson mass measurement*, *Phys. Rev. D* **88** (2013) 053005 [1306.5546].

[9] T. Blum, N. Christ, M. Hayakawa, T. Izubuchi, L. Jin, C. Jung et al., *Hadronic Light-by-Light Scattering Contribution to the Muon Anomalous Magnetic Moment from Lattice QCD*, *Phys. Rev. Lett.* **124** (2020) 132002 [1911.08123].

[10] E.-H. Chao, R. J. Hudspith, A. Gérardin, J. R. Green, H. B. Meyer and K. Ottnad, *Hadronic light-by-light contribution to* $(g-2)_\mu$ *from lattice QCD: a complete calculation*, *Eur. Phys. J. C* **81** (2021) 651 [2104.02632].

[11] E.-H. Chao, R. J. Hudspith, A. Gérardin, J. R. Green and H. B. Meyer, *The charm-quark contribution to light-by-light scattering in the muon* $(g-2)$ *from lattice QCD*, *Eur. Phys. J. C* **82** (2022) 664 [2204.08844].

[12] T. Blum, N. Christ, M. Hayakawa, T. Izubuchi, L. Jin, C. Jung et al., *Hadronic light-by-light contribution to the muon anomaly from lattice QCD with infinite volume QED at physical pion mass*, 2304.04423.

[13] S. J. Brodsky and E. De Rafael, *Suggested Boson-Lepton Pair Couplings and the Anomalous Magnetic Moment of the Muon*, *Phys. Rev.* **168** (1968) 1620.

[14] T. Aoyama et al., *The anomalous magnetic moment of the muon in the Standard Model*, *Phys. Rept.* **887** (2020) 1 [2006.04822].

[15] M. Davier, A. Hoecker, B. Malaescu and Z. Zhang, *Reevaluation of the hadronic vacuum polarisation contributions to the Standard Model predictions of the muon* $g-2$ *and* $\alpha(m_Z^2)$ *using newest hadronic cross-section data*, *Eur. Phys. J. C* **77** (2017) 827 [1706.09436].

[16] A. Keshavarzi, D. Nomura and T. Teubner, *The muon* $g-2$ *and* $\alpha(M_Z^2)$*: a new data-based analysis*, *Phys. Rev. D* **97** (2018) 114025 [1802.02995].

[17] G. Colangelo, M. Hoferichter and P. Stoffer, *Two-pion contribution to hadronic vacuum polarization*, *JHEP* **02** (2019) 006 [1810.00007].

[18] M. Hoferichter, B.-L. Hoid and B. Kubis, *Three-pion contribution to hadronic vacuum polarization*, *JHEP* **08** (2019) 137 [1907.01556].

[19] M. Davier, A. Hoecker, B. Malaescu and Z. Zhang, *A new evaluation of the hadronic vacuum polarisation contributions to the muon anomalous magnetic moment and to* $\alpha(m_Z^2)$, *Eur. Phys. J. C* **80** (2020) 241 [1908.00921].

[20] A. Keshavarzi, D. Nomura and T. Teubner, *The* $g-2$ *of charged leptons,* $\alpha(M_Z^2)$ *and the hyperfine splitting of muonium*, *Phys. Rev. D* **101** (2020) 014029 [1911.00367].

[21] A. Kurz, T. Liu, P. Marquard and M. Steinhauser, *Hadronic contribution to the muon anomalous magnetic moment to next-to-next-to-leading order*, *Phys. Lett. B* **734** (2014) 144 [1403.6400].

[22] CMD-3 collaboration, F. V. Ignatov et al., *Measurement of the* $e^+e^- \to \pi^+\pi^-$ *cross section from threshold to 1.2 GeV with the CMD-3 detector*, 2302.08834.

[23] G. Abbiendi et al., *Measuring the leading hadronic contribution to the muon g-2 via μe scattering*, *Eur. Phys. J. C* **77** (2017) 139 [1609.08987].

[24] D. Mohler, S. Schaefer and J. Simeth, *CLS 2+1 flavor simulations at physical light- and strange-quark masses*, *EPJ Web Conf.* **175** (2018) 02010 [1712.04884].

[25] RBC, UKQCD collaboration, T. Blum, P. A. Boyle, V. Gülpers, T. Izubuchi, L. Jin, C. Jung et al., *Calculation of the hadronic vacuum polarization contribution to the muon anomalous magnetic moment*, *Phys. Rev. Lett.* **121** (2018) 022003 [1801.07224].

[26] European Twisted Mass collaboration, D. Giusti, V. Lubicz, G. Martinelli, F. Sanfilippo and S. Simula, *Electromagnetic and strong isospin-breaking corrections to the muon* $g-2$ *from Lattice QCD+QED*, *Phys. Rev. D* **99** (2019) 114502 [1901.10462].

[27] PACS collaboration, E. Shintani and Y. Kuramashi, *Hadronic vacuum polarization contribution to the muon* $g-2$ *with 2+1 flavor lattice QCD on a larger than (10 fm)*^{4} *lattice at the physical point*, *Phys. Rev. D* **100** (2019) 034517 [1902.00885].

[28] Fermilab Lattice, HPQCD, MILC collaboration, C. T. H. Davies et al., *Hadronic-vacuum-polarization contribution to the muon's anomalous magnetic moment from four-flavor lattice QCD*, *Phys. Rev. D* **101** (2020) 034512 [1902.04223].

[29] A. Gérardin, M. Cè, G. von Hippel, B. Hörz, H. B. Meyer, D. Mohler et al., *The leading hadronic contribution to* $(g-2)_\mu$ *from lattice QCD with* $N_f = 2+1$ *flavours of O(a) improved Wilson quarks*, *Phys. Rev. D* **100** (2019) 014510 [1904.03120].

[30] S. Borsanyi et al., *Leading hadronic contribution to the muon magnetic moment from lattice QCD*, *Nature* **593** (2021) 51 [2002.12347].

[31] C. Lehner and A. S. Meyer, *Consistency of hadronic vacuum polarization between lattice QCD and the R-ratio*, *Phys. Rev. D* **101** (2020) 074515 [2003.04177].

[32] C. Aubin, T. Blum, M. Golterman and S. Peris, *Muon anomalous magnetic moment with staggered fermions: Is the lattice spacing small enough?*, *Phys. Rev. D* **106** (2022) 054503 [2204.12256].

[33] T. Blum, *Lattice calculation of the lowest order hadronic contribution to the muon anomalous magnetic moment*, *Phys. Rev. Lett.* **91** (2003) 052001 [hep-lat/0212018].

[34] D. Bernecker and H. B. Meyer, *Vector Correlators in Lattice QCD: Methods and applications*, *Eur. Phys. J. A* **47** (2011) 148 [1107.4388].

[35] M. Della Morte, A. Francis, V. Gülpers, G. Herdoíza, G. von Hippel, H. Horch et al., *The hadronic vacuum polarization contribution to the muon g − 2 from lattice QCD*, *JHEP* **10** (2017) 020 [1705.01775].

[36] HPQCD collaboration, B. Colquhoun, R. J. Dowdall, C. T. H. Davies, K. Hornbostel and G. P. Lepage, *Υ and Υ' Leptonic Widths, a_μ^b and m_b from full lattice QCD*, *Phys. Rev. D* **91** (2015) 074514 [1408.5768].

[37] M. Bruno, T. Izubuchi, C. Lehner and A. S. Meyer, *Exclusive Channel Study of the Muon HVP*, *PoS* **LATTICE2019** (2019) 239 [1910.11745].

[38] C. Lehner in *RBRC Workshop on Lattice Gauge Theories*, 2016, https://indico.bnl.gov/event/1628/contributions/2819/.

[39] Budapest-Marseille-Wuppertal collaboration, S. Borsanyi et al., *Hadronic vacuum polarization contribution to the anomalous magnetic moments of leptons from first principles*, *Phys. Rev. Lett.* **121** (2018) 022002 [1711.04980].

[40] S. Paul, A. D. Hanlon, B. Hörz, D. Mohler, C. Morningstar and H. Wittig, *The long-distance behaviour of the vector-vector correlator from $\pi\pi$ scattering*, *PoS* **LATTICE2022** (2023) 073.

[41] C. Andersen, J. Bulava, B. Hörz and C. Morningstar, *The $I = 1$ pion-pion scattering amplitude and timelike pion form factor from $N_f = 2 + 1$ lattice QCD*, *Nucl. Phys. B* **939** (2019) 145 [1808.05007].

[42] H. Neff, N. Eicker, T. Lippert, J. W. Negele and K. Schilling, *On the low fermionic eigenmode dominance in QCD on the lattice*, *Phys. Rev. D* **64** (2001) 114509 [hep-lat/0106016].

[43] L. Giusti, P. Hernandez, M. Laine, P. Weisz and H. Wittig, *Low-energy couplings of QCD from current correlators near the chiral limit*, *JHEP* **04** (2004) 013 [hep-lat/0402002].

[44] T. A. DeGrand and S. Schaefer, *Improving meson two point functions in lattice QCD*, *Comput. Phys. Commun.* **159** (2004) 185 [hep-lat/0401011].

[45] G. S. Bali, S. Collins and A. Schäfer, *Effective noise reduction techniques for disconnected loops in Lattice QCD*, *Comput. Phys. Commun.* **181** (2010) 1570 [0910.3970].

[46] T. Blum, T. Izubuchi and E. Shintani, *New class of variance-reduction techniques using lattice symmetries*, *Phys. Rev. D* **88** (2013) 094503 [1208.4349].

[47] E. Shintani, R. Arthur, T. Blum, T. Izubuchi, C. Jung and C. Lehner, *Covariant approximation averaging*, *Phys. Rev. D* **91** (2015) 114511 [1402.0244].

[48] M. Cè, L. Giusti and S. Schaefer, *Domain decomposition, multi-level integration and exponential noise reduction in lattice QCD*, *Phys. Rev. D* **93** (2016) 094507 [1601.04587].

[49] M. Cè, L. Giusti and S. Schaefer, *A local factorization of the fermion determinant in lattice QCD*, *Phys. Rev. D* **95** (2017) 034503 [1609.02419].

[50] M. Dalla Brida, L. Giusti, T. Harris and M. Pepe, *Multi-level Monte Carlo computation of the hadronic vacuum polarization contribution to* $(g_\mu - 2)$, *Phys. Lett. B* **816** (2021) 136191 [2007.02973].

[51] D. Giusti, F. Sanfilippo and S. Simula, *Light-quark contribution to the leading hadronic vacuum polarization term of the muon g − 2 from twisted-mass fermions*, *Phys. Rev. D* **98** (2018) 114504 [1808.00887].

[52] C. Aubin, T. Blum, C. Tu, M. Golterman, C. Jung and S. Peris, *Light quark vacuum polarization at the physical point and contribution to the muon g − 2*, *Phys. Rev. D* **101** (2020) 014503 [1905.09307].

[53] J. Bijnens and J. Relefors, *Vector two-point functions in finite volume using partially quenched chiral perturbation theory at two loops*, *JHEP* **12** (2017) 114 [1710.04479].

[54] C. Aubin, T. Blum, M. Golterman and S. Peris, *Application of effective field theory to finite-volume effects in* $a_\mu^{\rm HVP}$, *Phys. Rev. D* **102** (2020) 094511 [2008.03809].

[55] J. J. Sakurai, *Theory of strong interactions*, *Annals Phys.* **11** (1960) 1.

[56] F. Jegerlehner and R. Szafron, *$\rho^0 - \gamma$ mixing in the neutral channel pion form factor $F_\pi^{(e)}(s)$ and its role in comparing e^+e^- with τ spectral functions*, *Eur. Phys. J. C* **71** (2011) 1632 [1101.2872].

[57] HPQCD collaboration, B. Chakraborty, C. T. H. Davies, P. G. de Oliviera, J. Koponen, G. P. Lepage and R. S. Van de Water, *The hadronic vacuum polarization contribution to a_μ from full lattice QCD*, *Phys. Rev. D* **96** (2017) 034516 [1601.03071].

[58] M. Lüscher, *Volume Dependence of the Energy Spectrum in Massive Quantum Field Theories. 2. Scattering States*, *Commun. Math. Phys.* **105** (1986) 153.

[59] L. Lellouch and M. Lüscher, *Weak transition matrix elements from finite volume correlation functions*, *Commun. Math. Phys.* **219** (2001) 31 [hep-lat/0003023].

[60] H. B. Meyer, *Lattice QCD and the Timelike Pion Form Factor*, *Phys. Rev. Lett.* **107** (2011) 072002 [1105.1892].

[61] G. J. Gounaris and J. J. Sakurai, *Finite width corrections to the vector meson dominance prediction for $\rho \to e^+e^-$*, *Phys. Rev. Lett.* **21** (1968) 244.

[62] A. Francis, B. Jäger, H. B. Meyer and H. Wittig, *A new representation of the Adler function for lattice QCD*, *Phys. Rev. D* **88** (2013) 054502 [1306.2532].

[63] M. T. Hansen and A. Patella, *Finite-volume effects in $(g-2)_\mu^{\mathrm{HVP,LO}}$*, *Phys. Rev. Lett.* **123** (2019) 172001 [1904.10010].

[64] M. T. Hansen and A. Patella, *Finite-volume and thermal effects in the leading-HVP contribution to muonic $(g-2)$*, *JHEP* **10** (2020) 029 [2004.03935].

[65] M. Cè, T. Harris, H. B. Meyer, A. Toniato and C. Török, *Vacuum correlators at short distances from lattice QCD*, *JHEP* **12** (2021) 215 [2106.15293].

[66] R. Sommer, L. Chimirri and N. Husung, *Log-enhanced discretization errors in integrated correlation functions*, *PoS* **LATTICE2022** (2023) 358 [2211.15750].

[67] N. Husung, P. Marquard and R. Sommer, *Asymptotic behavior of cutoff effects in Yang–Mills theory and in Wilson's lattice QCD*, *Eur. Phys. J. C* **80** (2020) 200 [1912.08498].

[68] N. Husung, P. Marquard and R. Sommer, *The asymptotic approach to the continuum of lattice QCD spectral observables*, *Phys. Lett. B* **829** (2022) 137069 [2111.02347].

[69] N. Husung, *SymEFT predictions for local fermion bilinears*, *PoS* **LATTICE2023** (2024) 364 [2401.04303].

[70] M. Cè et al., *Window observable for the hadronic vacuum polarization contribution to the muon g-2 from lattice QCD*, *Phys. Rev. D* **106** (2022) 114502 [2206.06582].

[71] RBC, UKQCD collaboration, T. Blum et al., *Update of Euclidean windows of the hadronic vacuum polarization*, *Phys. Rev. D* **108** (2023) 054507 [2301.08696].

[72] Extended Twisted Mass collaboration, C. Alexandrou et al., *Lattice calculation of the short and intermediate time-distance hadronic vacuum polarization contributions to the muon magnetic moment using twisted-mass fermions*, *Phys. Rev. D* **107** (2023) 074506 [2206.15084].

[73] Flavour Lattice Averaging Group (FLAG) collaboration, Y. Aoki et al., *FLAG Review 2021*, *Eur. Phys. J. C* **82** (2022) 869 [2111.09849].

[74] G. Colangelo et al., *Data-driven evaluations of Euclidean windows to scrutinize hadronic vacuum polarization*, *Phys. Lett. B* **833** (2022) 137313 [2205.12963].

[75] D. Boito, M. Golterman, K. Maltman and S. Peris, *Spectral-weight sum rules for the hadronic vacuum polarization*, *Phys. Rev. D* **107** (2023) 034512 [2210.13677].

[76] M. Davier, Z. Fodor, A. Gerardin, L. Lellouch, B. Malaescu, F. M. Stokes et al., *Hadronic vacuum polarization: comparing lattice QCD and data-driven results in systematically improvable ways*, 2308.04221.

[77] G. Colangelo, *Data-driven approaches to the evaluation of hadronic contributions to the $(g-2)_\mu$*, *EPJ Web Conf.* **258** (2022) 01004.

[78] Extended Twisted Mass collaboration, C. Alexandrou et al., *Probing the Energy-Smeared R Ratio Using Lattice QCD*, *Phys. Rev. Lett.* **130** (2023) 241901 [2212.08467].

[79] D. Giusti and S. Simula, *Window contributions to the muon hadronic vacuum polarization with twisted-mass fermions*, *PoS* **LATTICE2021** (2022) 189 [2111.15329].

[80] H. Wittig, *Progress on $(g-2)_\mu$ from Lattice QCD*, in *57th Rencontres de Moriond on Electroweak Interactions and Unified Theories*, 6, 2023, 2306.04165.

[81] J. A. Miranda and P. Roig, *New τ-based evaluation of the hadronic contribution to the vacuum polarization piece of the muon anomalous magnetic moment*, *Phys. Rev. D* **102** (2020) 114017 [2007.11019].

[82] P. Masjuan, A. Miranda and P. Roig, *τ data-driven evaluation of Euclidean windows for the hadronic vacuum polarization*, 2305.20005.

[83] M. Davier, A. Hoecker, A. M. Lutz, B. Malaescu and Z. Zhang, *Tensions in $e^+e^- \to \pi^+\pi^-(\gamma)$ measurements: the new landscape of data-driven hadronic vacuum polarization predictions for the muon $g-2$*, 2312.02053.

[84] G. Benton, D. Boito, M. Golterman, A. Keshavarzi, K. Maltman and S. Peris, *Data-Driven Determination of the Light-Quark Connected Component of the Intermediate-Window Contribution to the Muon g-2*, *Phys. Rev. Lett.* **131** (2023) 251803 [2306.16808].

[85] H. B. Meyer, *Lorentz-covariant coordinate-space representation of the leading hadronic contribution to the anomalous magnetic moment of the muon*, *Eur. Phys. J. C* **77** (2017) 616 [1706.01139].

[86] E.-H. Chao, H. B. Meyer and J. Parrino, *Coordinate-space calculation of the window observable for the hadronic vacuum polarization contribution to (g-2)$_\mu$*, *Phys. Rev. D* **107** (2023) 054505 [2211.15581].

[87] A. Francis, P. Fritzsch, M. Lüscher and A. Rago, *Master-field simulations of O(a)-improved lattice QCD: Algorithms, stability and exactness*, *Comput. Phys. Commun.* **255** (2020) 107355 [1911.04533].

[88] chiQCD collaboration, G. Wang, T. Draper, K.-F. Liu and Y.-B. Yang, *Muon g-2 with overlap valence fermions*, *Phys. Rev. D* **107** (2023) 034513 [2204.01280].

[89] Fermilab Lattice, HPQCD, MILC collaboration, A. Bazavov et al., *Light-quark connected intermediate-window contributions to the muon g-2 hadronic vacuum polarization from lattice QCD*, *Phys. Rev. D* **107** (2023) 114514 [2301.08274].

[90] Budapest-Marseille-Wuppertal collaboration, S. Borsanyi et al., *Hadronic vacuum polarization contribution to the anomalous magnetic moments of leptons from first principles*, *Phys. Rev. Lett.* **121** (2018) 022002 [1711.04980].

[91] V. Gülpers, A. Francis, B. Jäger, H. Meyer, G. von Hippel and H. Wittig, *The leading disconnected contribution to the anomalous magnetic moment of the muon*, *PoS* **LATTICE2014** (2014) 128 [1411.7592].

[92] M. Della Morte and A. Jüttner, *Quark disconnected diagrams in chiral perturbation theory*, *JHEP* **1011** (2010) 154 [1009.3783].

[93] A. Stathopoulos, J. Laeuchli and K. Orginos, *Hierarchical Probing for Estimating the Trace of the Matrix Inverse on Toroidal Lattices*, *SIAM J. Sci. Comput.* **35** (2013) S299 [1302.4018].

[94] T. Blum, P. A. Boyle, T. Izubuchi, L. Jin, A. Jüttner, C. Lehner et al., *Calculation of the hadronic vacuum polarization disconnected contribution to the muon anomalous magnetic moment*, *Phys. Rev. Lett.* **116** (2016) 232002 [1512.09054].

[95] C. Thron, S. J. Dong, K. F. Liu and H. P. Ying, *Padé - Z(2) estimator of determinants*, *Phys. Rev. D* **57** (1998) 1642 [hep-lat/9707001].

[96] UKQCD collaboration, C. McNeile and C. Michael, *Decay width of light quark hybrid meson from the lattice*, *Phys. Rev. D* **73** (2006) 074506 [hep-lat/0603007].

[97] L. Giusti, T. Harris, A. Nada and S. Schaefer, *Frequency-splitting estimators of single-propagator traces*, *Eur. Phys. J. C* **79** (2019) 586 [1903.10447].

[98] M. Cè, A. Gérardin, G. von Hippel, H. B. Meyer, K. Miura, K. Ottnad et al., *The hadronic running of the electromagnetic coupling and the electroweak mixing angle from lattice QCD*, *JHEP* **08** (2022) 220 [2203.08676].

[99] A. Patella, *QED Corrections to Hadronic Observables*, *PoS* **LATTICE2016** (2017) 020 [1702.03857].

[100] M. Di Carlo, *Isospin-breaking and electromagnetic corrections to weak decays*, *PoS* **LATTICE2023** (2024) 120.

[101] A. Westin, W. Kamleh, R. Young, J. Zanotti, R. Horsley, Y. Nakamura et al., *Anomalous magnetic moment of the muon with dynamical QCD+QED*, *EPJ Web Conf.* **245** (2020) 06035.

[102] RCSTAR collaboration, L. Bushnaq, I. Campos, M. Catillo, A. Cotellucci, M. Dale, P. Fritzsch et al., *First results on QCD+QED with C^* boundary conditions*, *JHEP* **03** (2023) 012 [2209.13183].

[103] FERMILAB LATTICE, HPQCD, MILC collaboration, B. Chakraborty et al., *Strong-Isospin-Breaking Correction to the Muon Anomalous Magnetic Moment from Lattice QCD at the Physical Point*, *Phys. Rev. Lett.* **120** (2018) 152001 [1710.11212].

[104] G. M. de Divitiis et al., *Isospin breaking effects due to the up-down mass difference in lattice QCD*, *JHEP* **04** (2012) 124 [1110.6294].

[105] RM123 collaboration, G. M. de Divitiis, R. Frezzotti, V. Lubicz, G. Martinelli, R. Petronzio, G. C. Rossi et al., *Leading isospin breaking effects on the lattice*, *Phys. Rev. D* **87** (2013) 114505 [1303.4896].

[106] V. Biloshytskyi, E.-H. Chao, A. Gérardin, J. R. Green, F. Hagelstein, H. B. Meyer et al., *Forward light-by-light scattering and electromagnetic correction to hadronic vacuum polarization*, *JHEP* **03** (2023) 194 [2209.02149].

[107] E.-H. Chao, H. B. Meyer and J. Parrino, *Coordinate-space calculation of QED corrections to the hadronic vacuum polarization contribution to* $(g-2)_\mu$, in *40th International Symposium on Lattice Field Theory*, 10, 2023, 2310.20556.

[108] J. Green, O. Gryniuk, G. von Hippel, H. B. Meyer and V. Pascalutsa, *Lattice QCD calculation of hadronic light-by-light scattering*, *Phys. Rev. Lett.* **115** (2015) 222003 [1507.01577].

[109] N. Asmussen, J. Green, H. B. Meyer and A. Nyffeler, *Position-space approach to hadronic light-by-light scattering in the muon g − 2 on the lattice*, *PoS* **LATTICE2016** (2016) 164 [1609.08454].

[110] M. Hayakawa and S. Uno, *QED in finite volume and finite size scaling effect on electromagnetic properties of hadrons*, *Prog. Theor. Phys.* **120** (2008) 413 [0804.2044].

[111] J. Bijnens, J. Harrison, N. Hermansson-Truedsson, T. Janowski, A. Jüttner and A. Portelli, *Electromagnetic finite-size effects to the hadronic vacuum polarization*, *Phys. Rev. D* **100** (2019) 014508 [1903.10591].

[112] L. Polley and U. J. Wiese, *Monopole condensate and monopole mass in U(1) lattice gauge theory*, *Nucl. Phys.* **B356** (1991) 629.

[113] B. Lucini, A. Patella, A. Ramos and N. Tantalo, *Charged hadrons in local finite-volume QED+QCD with C^* boundary conditions*, *JHEP* **02** (2016) 076 [1509.01636].

[114] N. Tantalo, *Matching lattice QC+ED to Nature*, *PoS* **LATTICE2022** (2023) 249 [2301.02097].

[115] A. Gérardin, *The anomalous magnetic moment of the muon: status of lattice QCD calculations*, *Eur. Phys. J. A* **57** (2021) 116 [2012.03931].

[116] G. Ray et al., *Calculating the QED correction to the hadronic vacuum polarisation on the lattice*, *PoS* **LATTICE2022** (2023) 329 [2212.12031].

[117] T. Harris, V. Gülpers, A. Portelli and J. Richings, *Efficiently unquenching QCD+QED at* $O(\alpha)$, *PoS* **LATTICE2022** (2023) 013 [2301.03995].

[118] ALPHA collaboration, S. Schaefer, R. Sommer and F. Virotta, *Critical slowing down and error analysis in lattice QCD simulations*, *Nucl. Phys. B* **845** (2011) 93 [1009.5228].